Crystallography Reports, Vol. 49, Suppl. 1, 2004, pp. S80–S88.

REAL CRYSTAL STRUCTURE

Investigation of Structural Perfection and Acoustic Properties of $La_3Ga_5SiO_{14}$ Crystals by High Resolution X-Ray Diffraction, Topography, and Microfluorescence Analysis

D. V. Roshchupkin*, D. V. Irzhak, E. D. Roshchupkina***, and O. A. Buzanov*****

** Institute of Microelectronic Technology and Ultra-High-Purity Materials, Russian Academy of Sciences, Chernogolovka, Moscow oblast, 142432 Russia*

e-mail: rochtch@ipmt-hpm.ac.ru

*** Moscow Institute of Steel and Alloys, Leninskiĭ pr. 4, Moscow, 117936 Russia*

**** Fomos Materials, Moscow, Russia*

Received November 26, 2003

Abstract—Main types of growth defects—stripes, twins, mosaicity, amorphous inclusions, periodic modulation of the distributions of Ga and La atoms along the growth axis—are revealed in langasite crystals grown by the Czochralski method using high-resolution X-ray diffractometry, topography, and microfluorescence analysis. The specific features of the propagation of surface acoustic waves in different cuts of langasite crystals are studied. *© 2004 MAIK "Nauka/Interperiodica".*

INTRODUCTION

Intensive development of telecommunication systems based on acoustoelectric devices that process complex digital signals in real time (mobile telephones, pagers, GPS systems, and so on), requires new piezoelectric materials. Well-known piezoelectric crystals (SiO_2, $LiNbO_3$, $LiTaO_3$) do not correspond the new communication standards. Langasite ($La_3Ga_5SiO_{14}$, LGS) is a promising material for acoustoelectronics since it combines good acoustic properties of $LiNbO_3$ (high electromechanical-coupling coefficient) and quartz (some cuts of LGS have a zero frequency coefficient) [1, 2] Thus, LGS can be used to form acoustoelectric microdevices operating on surface and bulk acoustic waves [3–5].

The LGS structure is similar to the structure of trigonal quartz and has the following unit-cell parameters: a = 8.170 and c = 5.095 Å [6]. LGS crystals are grown by the Czochralski method [7–11]. During the crystal growth, several types of growth defects are formed, which deteriorate the propagation of acoustic waves in the crystals (ultrasound is scattered by structural defects and its propagation velocity changes). The formation of defects in LGS crystals is determined by both the blend and growth-atmosphere compositions and the temperature conditions during the growth. The following types of growth defects were revealed in LGS crystals by X-ray topography and transmission electron microscopy: decorated color centers, stripes, and amorphous glassy inclusions [8, 11, 12]. Note that it is most expedient to use X-ray diffraction to study structural defects since this technique is sensitive to defect-induced lattice distortions [13].

The purpose of this study is to investigate the perfection of the LGS crystal structure and the effect of growth defects on the propagation of surface acoustic waves (SAWs) in LGS by X-ray diffraction, topography, and microfluorescence analysis.

We investigated 4-inch LGS crystals grown by the Czochralski method in the FOMOS Materials. Figure 1 shows the photograph of an LGS crystal grown in the {011} direction.

SPECIFIC FEATURES OF INTERACTION OF X-RAY RADIATION WITH LGS CRYSTALS

LGS crystals are a complex object of study for X-ray measurements which is due to the presence of the

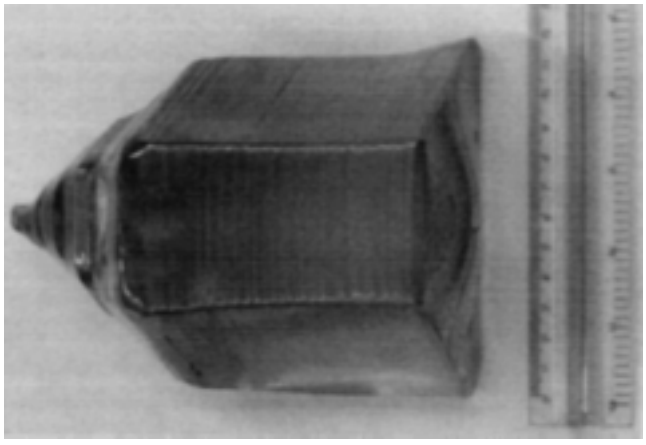

Fig. 1. 4-inch LGS crystal grown along the {011} axis.

1063-7745/04/4901-S0080$26.00 © 2004 MAIK "Nauka/Interperiodica"

La *L*-absorption edge and Ga *K*-absorption edge. The linear absorption coefficient of LGS is high, which results in a very short penetration depth of X-rays in LGS crystals. The kinematic theory of diffraction shows that the penetration depth of X-rays in a crystal is related to the absorptance in the form of a function of the X-ray energy *E*:

$$\mu^{-1}(E) = \sin(\theta_B(E))/2\mu_l(E), \quad (1)$$

where μ_l is the linear absorption coefficient and θ_B is the Bragg angle of incidence of X-rays.

Figure 2 shows the penetration depth of X-rays in LGS as a function of the X-ray energy, $\mu^{-1}(E)$, calculated from expression (1) for a number of successive reflections from *X* and *Y* cuts. The presence of the La *L* edge at an energy of 6 keV and the Ga *K* edge at an energy of 10.5 keV results in jumps in the X-ray absorption in these regions. As can be seen from Fig. 2, the use of Cu radiation with an energy of 8.048 keV makes it possible to investigate only a very thin (<1 μm) surface layer of a crystal. Hence, the structural perfection of LGS crystals was studied using Mo radiation with an energy of 17.479 keV, for which the penetration depth of X-rays in LGS is several micrometers.

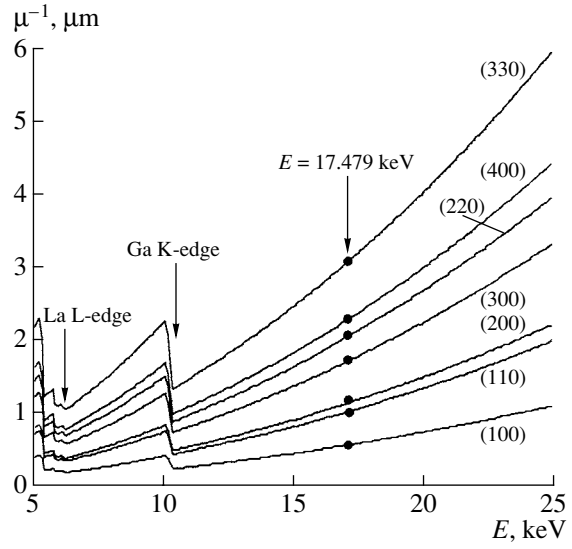

Fig. 2. Dependences of the penetration depth of X-rays in LGS on the X-ray energy.

SCHEMATIC OF THE EXPERIMENT

The structural perfection of LGS crystals was studied on a high-resolution double-crystal X-ray diffractometer (Fig. 3). A Rigaku Rotoflex Ru-200 X-ray tube with a rotating Mo anode was used as an X-ray source. The horizontal and vertical dimensions of the X-ray source were 10 μm and 10 mm, respectively. X-rays were collimated by the 10-μm entrance slit and monochromized by a double Si(111) monochromator crystal. After the monochromator crystal, MoK_{α_1} radiation (λ = 0.7093 Å) is incident on a crystal under study at the Bragg angle θ_B. A Kodak Electron SO-163 film with a grain size of 1 μm was used to record X-ray topograms. To obtain an image of a crystal, the film was mounted parallel to the crystal surface. Since the X-ray source was 10 μm in size, the crystal and the X-ray film were shifted simultaneously with respect to the source to obtain an image of the crystal surface of a larger area.

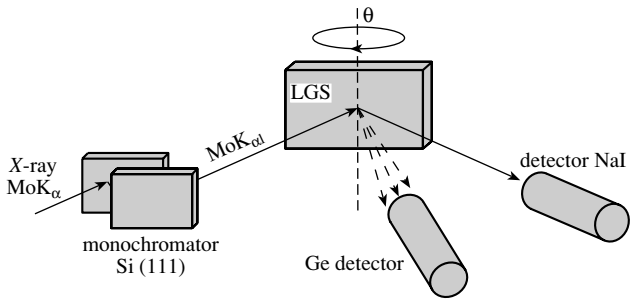

Fig. 3. Schematic of a high-resolution double-crystal X-ray diffractometer.

Fig. 4. X-ray topogram of concentric stripes. (022) reflection, θ_B = 9.879°.

X-ray diffraction permits integral estimation of the perfection of a crystal structure. To measure rocking curves, a Cyberstar Nal scintillation detector was installed in the exact Bragg position and θ scanning of the crystals was performed.

When studying the homogeneity of crystals along the growth axis, a solid-state Ge detector was used to measure the distribution of the fluorescent yield of Ga and La along the crystal growth axis upon scanning the X-ray beam over the crystal surface. To perform a local analysis, the X-ray beam was additionally collimated: the horizontal and vertical beam dimensions were, respectively, 5 and 100 μm in this case.

X-RAY TOPOGRAPHY OF LGS CRYSTALS

The LGS crystals grown by the Czochralski method along the {011} and {001} axes were investigated by high-resolution X-ray topography.

Figure 4 shows the topogram of a transverse cut of a 4-inch LGS crystal grown in the {011} direction. The topogram was recorded for the (022) reflection at the Bragg angle θ_B = 9.879°. Concentric stripes can be

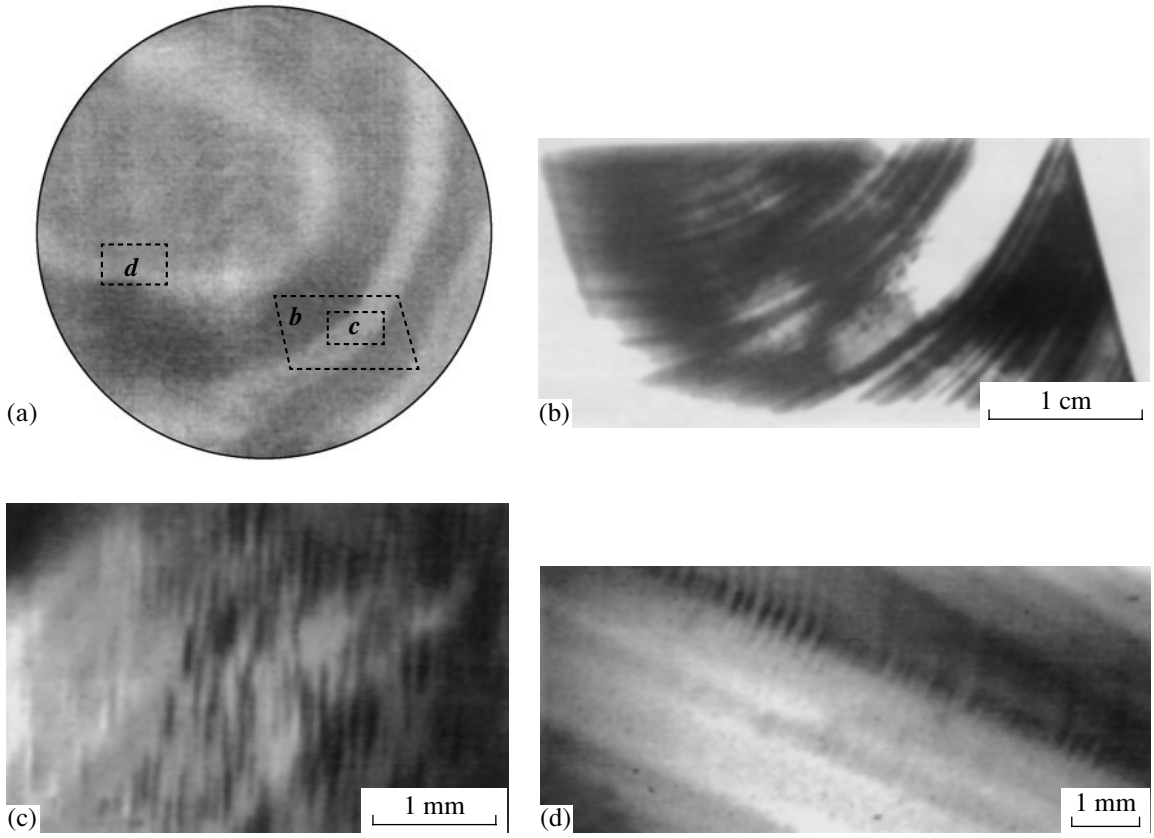

Fig. 5. 76-mm wafer in the *YXlt*/48.5°/26.6° cut of an LGS crystal: (a) optical image; (b) stripes; (c) mosaicity; (d) periodic deformations. (022) reflection, $\theta_B = 9.879°$.

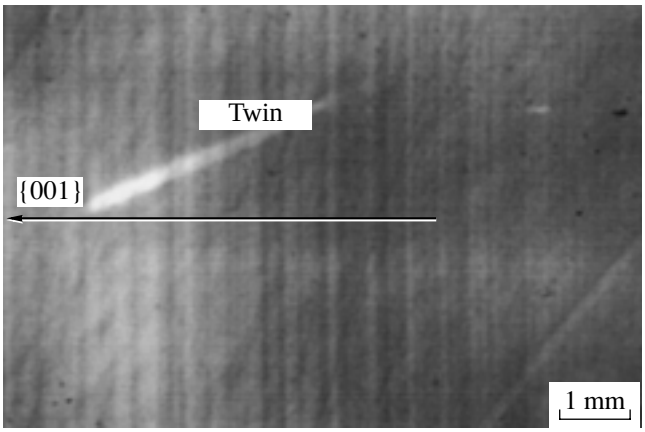

Fig. 6. X-ray topogram of the *X* cut of an LGS crystal. (330) reflection, $\theta_B = 15.101°$.

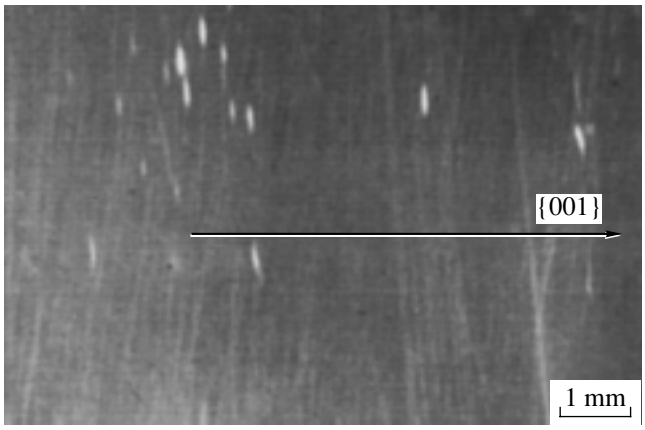

Fig. 7. X-ray topogram of amorphous inclusions in the initial growth part of an LGS crystal. (330) reflection, $\theta_B = 15.101°$.

observed on the topogram. Generally, stripes are perpendicular to the growth axis, but, for crystals of large diameter, the crystallization front has a spherical shape, which leads to the formation of stripes repeating the shape of the crystallization front.

Figure 5 shows the results of measurements for a 76-mm wafer in the *YXlt*/48.5°/26.6° cut of an LGS crystal. This cut is characterized by a zero frequency coefficient; it is used in production of SAW devices. The wafer was cut from a crystal grown in the {011} direction. Decorated areas of color centers can be seen in the optical image of the wafer (Fig. 5a). The areas from which X-ray topograms were measured for the (022) reflection are marked in Fig. 5a. The topogram in

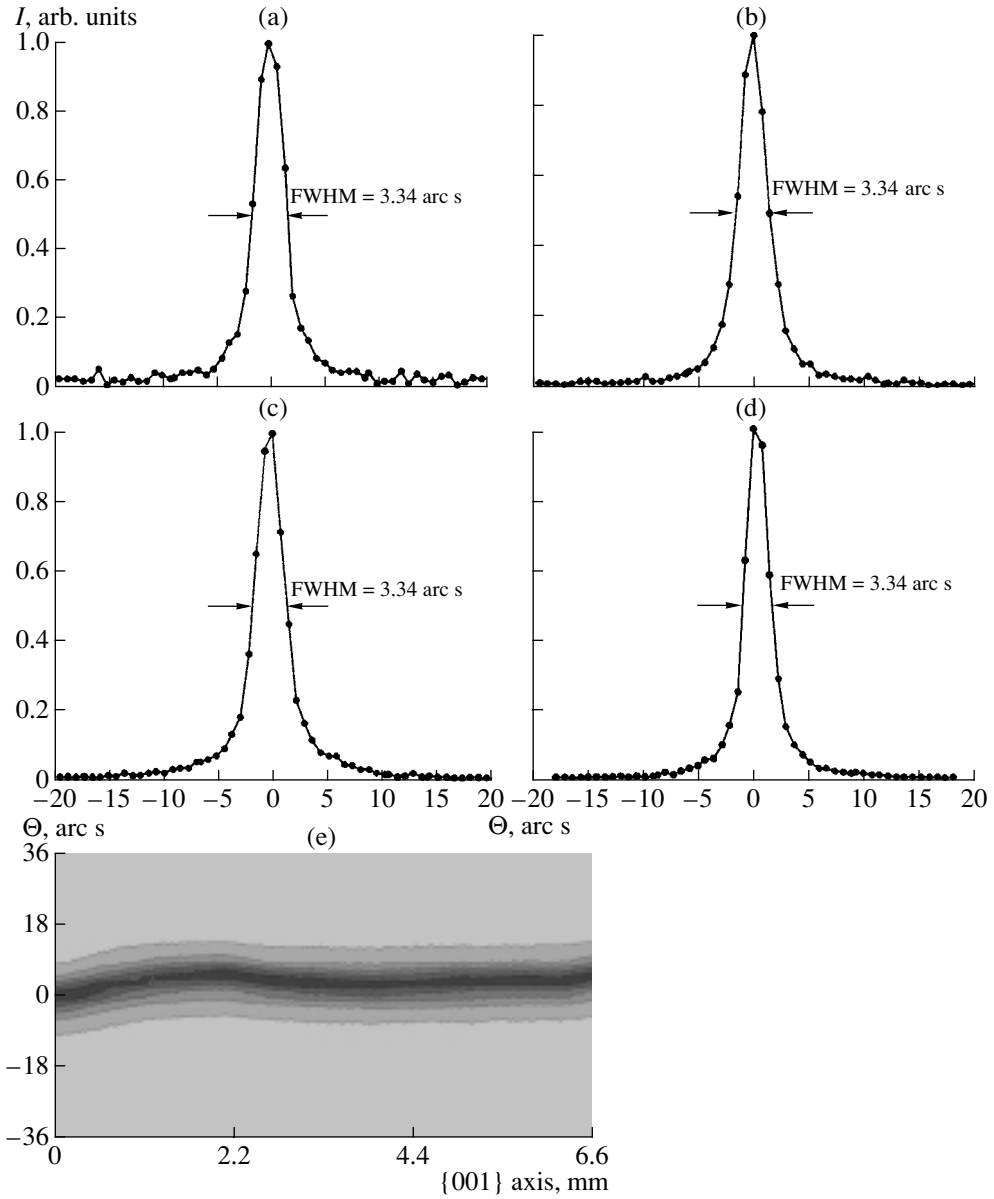

Fig. 8. Rocking curves for the *Y* cut of an LGS crystal: (a) (100) reflection, $\theta_B = 2.874°$; (b) (200) reflection, $\theta_B = 5.755°$; (c) (300) reflection, $\theta_B = 8.650°$; and (d) (400) reflection, $\theta_B = 11.569°$. (e) X-ray map along the growth axis {001}; (300) reflection.

Fig. 5b contains a bright area corresponding to the area of color centers in the optical photograph. The difference in the contrast is related to the change in the interplane distances due to the presence of color centers. In addition, stripes outgoing to the crystal surface can be observed in the topogram. Note that the brighter area is characterized by the presence of mosaicity with linear sizes of mosaic blocks of 30×500 μm^2 (Fig. 5c). The topogram obtained for the boundary of the decorated regions (Fig. 5d) shows the presence of periodic modulation of the crystal structure, which is caused by elastic strains at the interface between the two regions with different interplane distances.

The topogram of the *X* cut of the crystal grown in the {001} direction was obtained for the (330) reflection at the Bragg angle $\theta = 15.101°$. Transverse stripes with a period of about 145 μm can be seen on the topogram, as well as a twin in the form of a parallelepiped. This twin has a brighter contrast due to the deviation of its planes from the reflecting position. The angle between this twin and the growth axis {001} is 30°. The twin begins to grow into the crystal from the boundary of the stripe region. It is noteworthy that twins are often observed on X-ray topograms of LGS crystals.

On the topogram of the wafer cut from the crystal part grown in the initial stage, amorphous glassy inclusions can be seen, which do not reflect X-rays. They

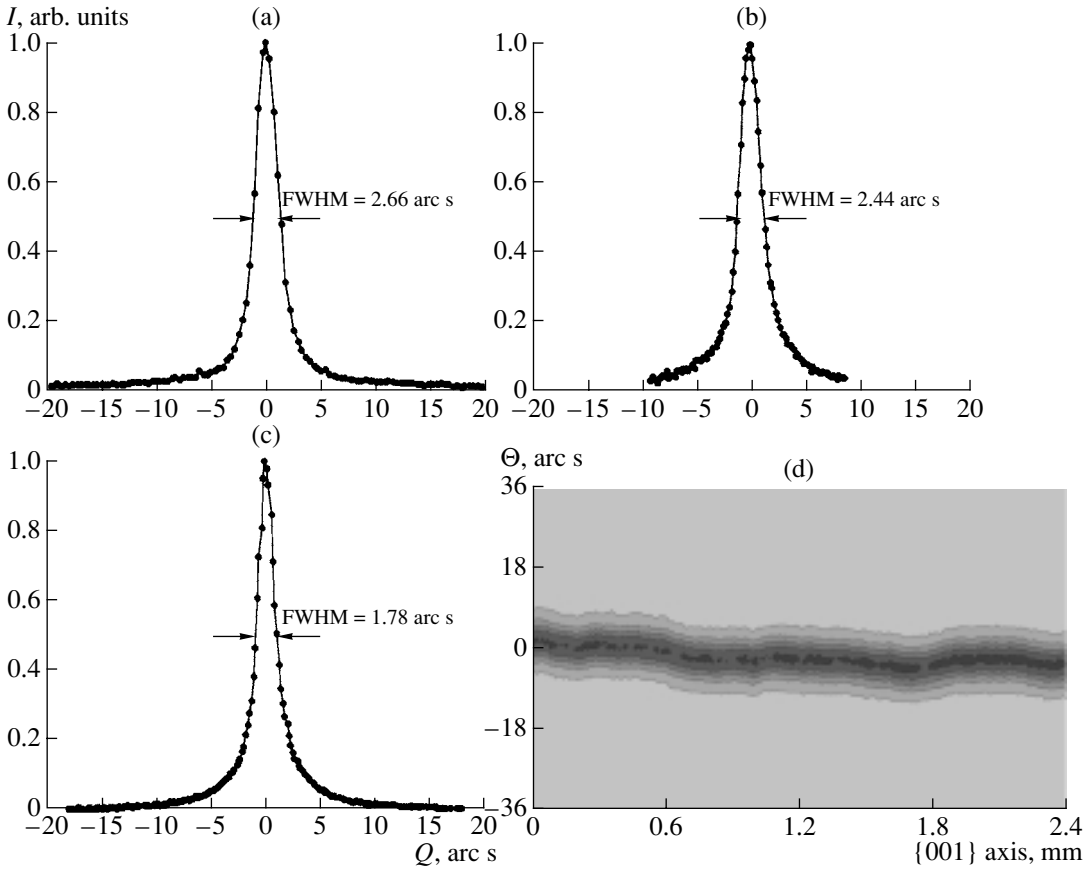

Fig. 9. Rocking curves for the *X* cut of an LGS crystal: (a) (110) reflection, $\theta_B = 4.982°$; (b) (220) reflection, $\theta_B = 10.002°$; and (c) (330) reflection, $\theta_B = 15.101°$. (d) X-ray map along the growth axis {001}; (330) reflection.

have a lens shape and are perpendicular to the growth axis.

HIGH-RESOLUTION X-RAY DIFFRACTION IN LGS CRYSTALS

High-resolution X-ray diffraction based on measuring the full width at half maximum (FWHM) of rocking curves makes it possible to analyze the degree of perfection of real crystals. Rocking curves are measured using θ scanning of crystals under study near the Bragg peak and the diffracted radiation is measured by a scintillation detector located at the exact Bragg position (Fig. 3).

The rocking curves for the *Y* cut of an LGS crystal for the (100), (200), (300), and (400) reflections are shown in Fig. 8. The FWHM values for these curves are $FWHM_{(100)} = 3.34$ arc s, $FWHM_{(200)} = 3.00$ arc s, $FWHM_{(300)} = 3.11$ arc s, and $FWHM_{(400)} = 2.67$ arc s. The small FWHM values of LGS crystals ensure a high contrast for growth defects when X-ray topography is used. Since the X-ray-beam size was 10 μm by 10 mm in our experiment, the measurement of the rocking curves was local. Thus, to study the structural perfection of a crystal, one should measure rocking curves from its different parts. Figure 8e shows the X-ray map measured along the growth axis {001} for the (300) reflection. The X-ray beam was scanned over the crystal surface with a step of 10 μm and 661 rocking curves were measured to plot a map along the growth axis. It can be seen from Fig. 8e that the diffraction maximum is slightly shifted along the growth axis, which is due to the change in the interplane distance $d_{(300)}$ along this axis. The maximum deviation of the Bragg peak position was $\Delta\theta = 2.5$ arc s at a distance of 6.6 mm along the growth axis, which corresponds to the relative variation in the interplane distance $\Delta d_{(300)}/d_{(300)} \approx 8 \times 10^{-5}$.

Similar investigations were also performed for the *X* cut of the LGS crystal (Fig. 9), where the rocking curves were measured for the (110), (220), and (330) reflections. The corresponding FWHM values were $FWHM_{(110)} = 2.66$ arc s, $FWHM_{(220)} = 2.44$ arc s, and $FWHM_{(330)} = 1.78$ arc s. Figure 9d shows the X-ray map along the growth axis {001} measured for the (330) reflection. The X-ray beam was scanned over the crystal surface with a step of 10 μm, and 241 rocking curves were measured to plot a map along the growth axis. In this case, the Bragg peak is also slightly shifted along the growth axis, which is due to the change in the interplane distance $d_{(330)}$. The maximum deviation of

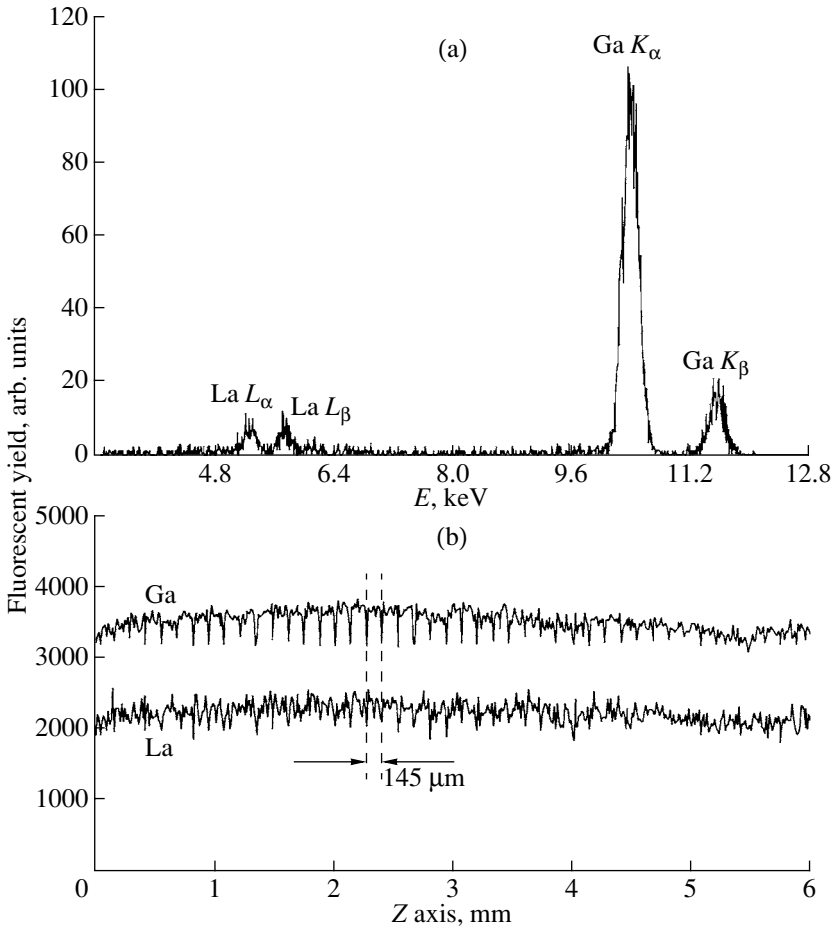

Fig. 10. (a) Fluorescent yield of an LGS crystal and (b) the distributions of the fluorescent yields LaL_α and GaK_α along the growth axis {001}.

the Bragg peak position is $\Delta\theta = 5.0$ arc s at a distance of 2.4 mm along the growth axis, which corresponds to $\Delta d_{(330)}/d_{(330)} \approx 9 \times 10^{-5}$.

Thus, the measured rocking curves demonstrate high structural perfection of the LGS crystals.

STUDY OF THE DISTRIBUTION OF La AND Ga ATOMS ALONG THE GROWTH AXIS OF AN LGS CRYSTAL BY MICROFLUORESCENCE ANALYSIS

The composition of an LGS crystals along their growth axes was studied by X-ray microfluorescence analysis in the *X* cut. The corresponding topogram is shown in Fig. 6. The X-ray beam was 5×100 μm in size and the angle of incidence of X-rays on the crystal was 45°. In this case, the projection of the X-ray beam on the crystal surface is 7×100 μm (7 μm correspond to the growth direction). X-rays with the energy E = 17.479 keV (Mo$K_{\alpha 1}$) excites the La L fluorescence (6 keV) and Ga K fluorescence (10.47 keV). Figure 10a shows the fluorescent yield of an LGS crystal recorded by a solid-state Ge detector located parallel to the crystal surface. The fluorescent yields LaL_α and GaK_α (Fig. 10b) were used to investigate the distribution of La and Ga atoms in the LGS crystal along its growth axis. With this purpose, the X-ray beam was scanned along the growth axis (i.e., perpendicular to the stripes).

As can be seen from Fig. 10b, the distributions of the fluorescent yields LaL_α and GaK_α are synchronously modulated along the growth axis with a period of 145 μm, which corresponds to the period of stripes on the topogram in Fig. 6. The result obtained demonstrates that the La and Ga concentrations synchronously drop at the interface between neighboring stripes.

VISUALIZATION OF ACOUSTIC WAVE FIELDS IN LGS CRYSTALS BY X-RAY TOPOGRAPHY

Generally, SAW propagation in crystals is studied by X-ray diffraction [14–15] and topographic [16–18] methods. X-ray diffraction measurements make it possible to determine the SAW amplitude and analyze the SAW decay along the propagation direction and over the crystal depth. X-ray topographic methods visualize

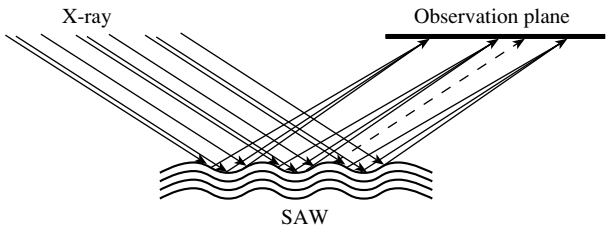

Fig. 11. Schematic diagram of the SAW-image formation by X-ray topography.

the SAW field on a crystal surface. In order to visualize a running SAW, one should synchronize the SAW excitation with the time characteristics of the synchrotron radiation, which significantly hinders the experiments and limits the frequency range of acoustoelectric devices that can be studied by X-ray topography [16–17]. In contrast to running SAWs, there is a real possibility of studying devices based on standing SAWs in all the frequency range using both laboratory and synchrotron X-ray sources [18].

The principle of visualization of a standing SAW is shown schematically in Fig. 11. It is based on focusing X-rays by a standing SAW. The nodes of a standing SAW are immobile and are located in the crystal surface plane, while antinodes serve as concave focusing mirrors and perform alternating focusing of X-rays in the observation plane located at a distance D from the crystal surface. The value of D can be determined from the expression:

$$D = \sin\theta_B/2hK^2(\sin^2\theta_B\sin^2\beta + \cos^2\beta), \qquad (2)$$

where θ_B is the Bragg angle, h is the SAW amplitude, $K = 2\pi/\Lambda$ is the SAW wave vector, Λ is the SAW wavelength, and β is the angle between the projection of the X-ray wave vector on the crystal surface and the SAW wave vector. When $\beta = 0$, expression (2) is significantly simplified:

$$D = \Lambda^2\sin^2\theta_B/8\pi^2h. \qquad (3)$$

As can be seen from expressions (2) and (3), it is most expedient to use large reflection indices and soft

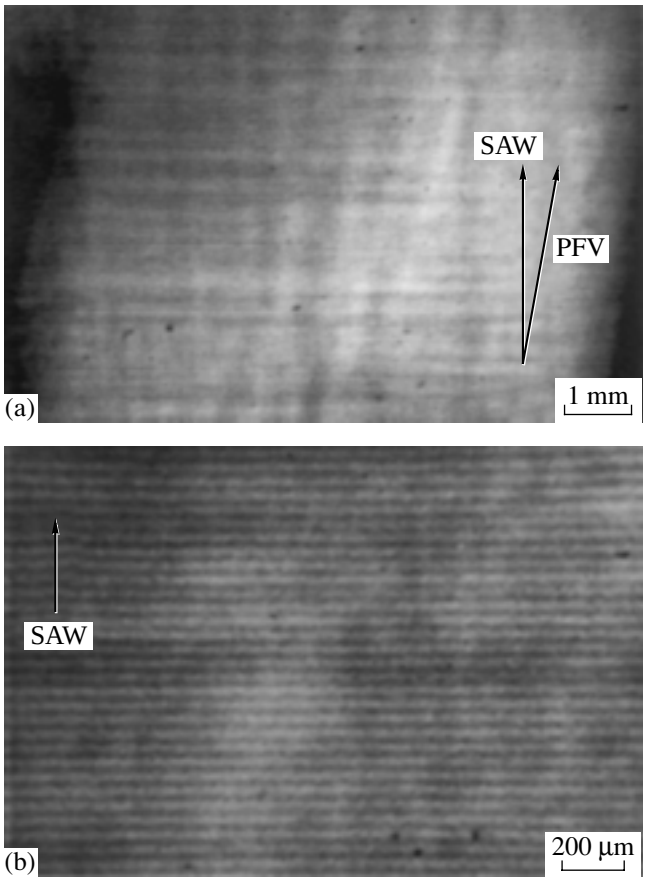

Fig. 12. X-ray topograms of the X cut of an LGS crystal excited by a standing SAW: (a) Fresnel diffraction pattern in an acoustic beam and (b) image of the standing SAW. (220) reflection, $\theta_B = 22.142°$, $\Lambda = 100$ μm, $f = 23.5$ MHz, $D = 5$ cm, and $h = 9.5$ Å.

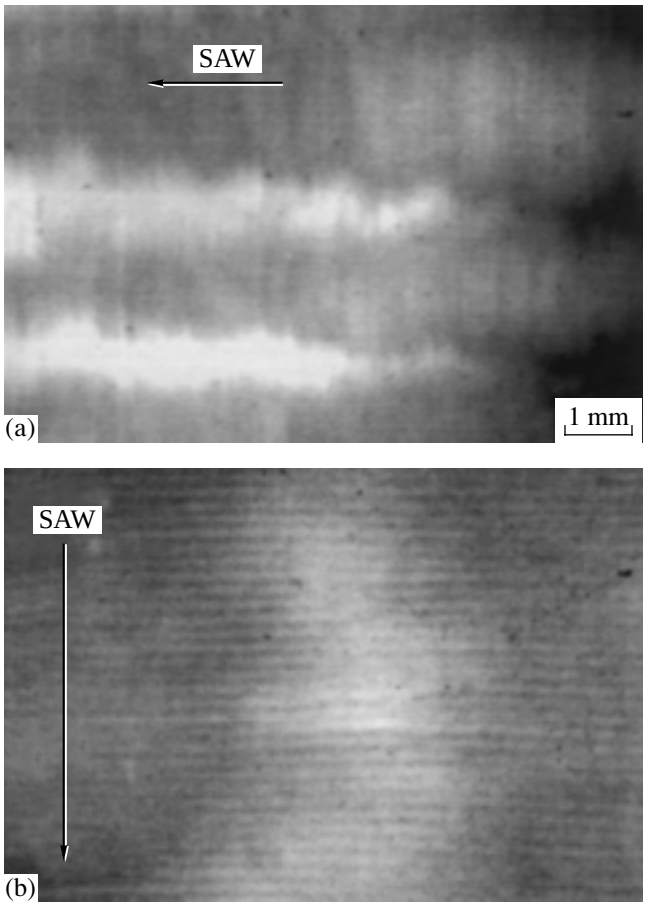

Fig. 13. X-ray topograms of the Y cut of an LGS crystal excited by a standing SAW: (a) acoustic wave field and (b) image of the distortion of the standing SAW wavefront. (300) reflection, $\theta_B = 19.008°$, $\Lambda = 100$ μm, $f = 23.1$ MHz, $D = 6$ cm, and $h = 6.9$ Å.

X-rays to simplify the experimental conditions for visualization of acoustic wave fields. Thus, we used Cu$K_{\alpha 1}$ radiation (E = 8.048 keV) for visualization of the standing-SAW fields in the X and Y cuts of LGS crystals. The period in the obtained image of a standing SAW in two times smaller than the SAW wavelength, since one wavelength of a standing SAW contains two nodes and two antinodes. To excite standing SAWs, we formed cavity structures on the crystal surfaces by photolithography. Each such structure consists of an interdigital transducer and two reflecting gratings. The interdigital transducer has the following parameters: the aperture W = 8 mm, the number of electrode pairs N = 40, and the SAW wavelength Λ = 100 μm. The field of a standing SAW is formed as a result of the interference between a running SAW excited by the interdigital transducer and the SAW reflected from the gratings.

Figure 12 shows the X-ray topograms of the X cut of an LGS crystal modulated by a standing SAW at the resonance excitation frequency f = 23.5 MHz. The SAW propagation velocity in this cut is v = 2350 m/s. The measurements were performed for the (220) reflection at the Bragg angle θ_B = 22.142°. The distance between the X-ray film and the sample surface is D = 5 cm. The topogram in Fig. 12 shows a Fresnel diffraction pattern in the acoustic beam, which is due to the SAW diffraction at the aperture of the interdigital transducer. The difference in the directions of the SAW wave vector and the acoustic power flow vector (PFV) can also be seen on the topogram in Fig. 12a. The drift angle of the acoustic power flow was 6.4°. Figure 12b shows the X-ray topogram of a standing-SAW image. The dark and bright fringes on the topogram correspond, respectively, to antinodes and nodes of the standing SAW. The period of the observed periodic structure is equal to 50 μm, which corresponds to a half of the SAW wavelength. Using the parameters of the experiment performed (D, Λ, θ_B) and expression (3), we can find the SAW amplitude. For the topograms shown in Fig. 12, the calculated value of the SAW amplitude is h = 9.5 Å.

Figure 13 shows the X-ray topograms of the Y cut of an LGS crystal modulated by a standing SAW. The resonance frequency of SAW excitation was f = 23.1 MHz at the SAW propagation velocity v = 2310 m/s. For the Y cut, the direction of the acoustic power flow coincides with the direction of the SAW wave vector. The topographic measurements were performed for the (300) reflection at the Bragg angle θ_B = 19.008°. The topograms were recorded at the distance D = 6 cm from the crystal surface, which corresponds to the SAW amplitude h = 6.9 Å. The difference in the contrast on the topogram shown in Fig. 13a is related to the presence of growth defects in the crystal. The bright contrast corresponds to the regions with color centers. Figure 13b shows a distortion of the SAW wavefront, which is due to the difference in the propagation velocities in the regions showing bright and dark contrasts in Fig. 13a. As can be seen from the topogram in Fig. 13b, growth defects affect significantly the process of SAW propagation.

CONCLUSIONS

Structural perfection and acoustic properties of LGS crystals grown by the Czochralski method in FOMOS Materials were investigated by the methods of high-resolution X-ray topography, diffractometry, and microfluorescence analysis.

High-resolution X-ray topography revealed the following main types of growth defects in LGS crystals: stripes, twins, amorphous inclusions, mosaicity, and elastic deformations at the boundaries of the regions of color centers.

Rocking curves for different reflections in the X and Y cuts of LGS crystal were measured on a double-crystal X-ray diffractometer. It has been shown that the FWHM of the rocking curves is very small; hence, LGS crystals can be used as monochromators for laboratory and synchrotron X-ray sources. Moreover, narrow rocking curves permit to obtain high-contrast images of growth defects in LGS crystals by X-ray topography.

X-ray microfluorescence analysis was used to investigate the distribution of La and Ga atoms along the growth axis in LGS crystals. It has been ascertained that the concentrations of La and Ga atoms are synchronously modulated along the growth axis; the modulation period corresponds to the period of the stripes. It is shown that the La and Ga concentrations drop at the stripe boundaries. Study of the propagation of standing SAWs in the X and Y cuts of an LGS crystal by X-ray topography made it possible to observe diffraction phenomena in acoustic beams, determine the drift angles for acoustic power flows and the SAW amplitudes, and to visualize the effect of growth defects on the SAW propagation.

ACKNOWLEDGMENTS

This study was supported by the Russian Foundation for Basic Research, project no. 02-02-22006.

REFERENCES

1. M. Kadota, J. Nakanishi, and T. Kumatoriya, Jpn. J. Appl. Phys. **38**, 3288 (1999).
2. S. Uda, A. Bunga, and C. Jian, Jpn. J. Appl. Phys. **38**, 5516 (1999).
3. M. P. Cunda and S. A. Fagundes, IEEE Trans. Sonics Ultrason. **46**, 1583 (1999).
4. M. Adachi, T. Karaki, and W. Miyamoto, Jpn. J. Appl. Phys. **38**, 3283 (1999).
5. N. Onozato, M. Adachi, and T. Karaki, Jpn. J. Appl. Phys. **39**, 3028 (2000).
6. E. Chilla, C. M. Flannery, H.-J. Frohlich, and U. Straube, J. Appl. Phys. **90**, 6084 (2001).
7. J. Bohm, R. B. Heimann, M. Hengst, *et al.*, J. Cryst. Growth **204**, 128 (1999).

8. S. Uda, A. Bungo, and C. Jian, Jpn. J. Appl. Phys. **38**, 5516 (1999).
9. I. H. Jung and K. H. Auh, Mater. Lett. **41**, 241 (1999).
10. S. Uda and O. Buzanov, J. Cryst. Growth **211**, 318 (2001).
11. H. Sato, M. Kumatoriya, and T. Fujii, J. Cryst. Growth **242**, 177 (2002).
12. R. Fachberger, T. Holzheu, E. Riha, *et al.*, in *Proceedings of IEEE International Frequency Control Symposium* (2001), p. 235.
13. D. K. Bowen and B. K. Tanner, *High Resolution X-ray Diffraction and Topography* (Taylor and Francis, London, 1998).
14. R. Tucoulou, F. De Bergevin, O. Mathon, and D. V. Roshchupkin, Phys. Rev. B **64**, 134 108 (2001).
15. D. V. Roshchupkin, D. V. Irzhak, R. Tucoulou, and O. A. Buzaniv, J. Appl. Phys. **94**, 6692 (2003).
16. H. Cerva and W. Graeff, Phys. Status Solidi A **82**, 35 (1984).
17. D. V. Roshchupkin, D. V. Irzhak, R. Tukulu, and O. Maton, Poverkhnost, No. 2, 27 (2003).
18. D. V. Irzhak and D. V. Roshchupkin, Poverkhnost, No. 1, 36 (2002).

Translated by Yu. Sin'kov

SPELL: ok